Draft version January 15, 2015
Preprint typeset using LaTeX style emulateapj v. 5/2/11

A NEARBY M STAR WITH THREE TRANSITING SUPER-EARTHS DISCOVERED BY K2

Ian J. M. Crossfield[1], Erik Petigura[2], Joshua Schlieder[3,12], Andrew W. Howard[4], B.J. Fulton[4], Kimberly M. Aller[4], David R. Ciardi[5], Sébastien Lépine[6], Thomas Barclay[3], Imke de Pater[2], Katherine de Kleer[2], Elisa V. Quintana[3], Jessie L. Christiansen[5], Eddie Schlafly[7], Lisa Kaltenegger[11], Justin R. Crepp[8], Thomas Henning[7], Christian Obermeier[7], Niall Deacon[9], Brad M. S. Hansen[10], Michael C. Liu[4], Tom Greene[3], Steve B. Howell[3], Travis Barman[1], Christoph Mordasini[7]

Draft version January 15, 2015

ABSTRACT

Small, cool planets represent the typical end-products of planetary formation. Studying the architectures of these systems, measuring planet masses and radii, and observing these planets' atmospheres during transit directly informs theories of planet assembly, migration, and evolution. Here we report the discovery of three small planets orbiting a bright ($K_s = 8.6$ mag) M0 dwarf using data collected as part of K2, the new ecliptic survey using the re-purposed *Kepler* spacecraft. Stellar spectroscopy and K2 photometry indicate that the system hosts three transiting planets with radii 1.5 – 2.1 $R_\oplus$, straddling the transition region between rocky and increasingly volatile-dominated compositions. With orbital periods of 10–45 days the planets receive just 1.5–10×the flux incident on Earth, making these some of the coolest small planets known orbiting a nearby star; planet d is located near the inner edge of the system's habitable zone. The bright, low-mass star makes this system an excellent laboratory to determine the planets' masses via Doppler spectroscopy and to constrain their atmospheric compositions via transit spectroscopy. This discovery demonstrates the power of K2 and future space-based transit searches to find many fascinating objects of interest.

Subject headings: EPIC 201367065— techniques: photometric — techniques: spectroscopic — eclipses

1. INTRODUCTION

Surveys for new planets demonstrate that small, low-mass planets are common around FGK stars (Howard et al. 2010, 2012). Petigura et al. (2013) used *Kepler* data to measure the frequency of Earth-sized planets in Earth-like orbits to be 5–20%. Such small planets with moderate insolation levels (the stellar energy received by the planet at the top of any atmosphere) are of considerable interest for their ability to host Earth-like atmospheres that could potentially support life.

M dwarfs offer a shortcut to observing rocky and potentially habitable planets. Compared to nearby Sunlike stars, planets around M dwarfs are easier to find with transits or radial velocities (RV), they occur more frequently (Howard et al. 2012), and their atmospheres are easier to study when transiting (Stevenson et al. 2010; Kreidberg et al. 2014). Planets transiting M dwarfs offer the best opportunity to study habitability and constrain models of rocky planet assembly and migration (Swift et al. 2013; Hansen 2014) and of planetary atmospheres (Kaltenegger et al. 2011; Rodler & López-Morales 2014). Multi-planet M dwarf systems are even more exciting, both because such candidates are extremely unlikely to result from astrophysical false positives (Lissauer et al. 2012) and because they allow for studies of comparative planetology (Muirhead et al. 2012) with identical initial conditions (i.e., formation in the same natal disk). However, relatively few confirmed transiting planets (and fewer multiple systems) are known around M dwarfs, and the (because *Kepler*'s prime mission targeted just 3900 late-type dwarfs) the prevalence of planets around M dwarfs is less well constrained than around Sunlike stars (Dressing & Charbonneau 2013).

We are using K2, the continuing mission of NASA's *Kepler* spacecraft (Howell et al. 2014), to target thousands of M dwarfs in each K2 field to find new, small planets orbiting these stars. K2's 80-day campaigns are ideally suited to finding large numbers of small, cool planets around M dwarfs, out to semimajor axes in the stars' habitable zones. In addition, some of K2's M-dwarf planets orbit stars bright enough for atmospheric characterization via JWST transmission or emission spectroscopy (Kaltenegger & Traub 2009; Batalha et al. 2013; Beichman et al. 2014).

Here, we present the discovery of a new multi-planet system orbiting a bright M dwarf (EPIC 201367065, PMI11293-0127, UCAC4 443-054906, PPMX 112920.3-012717). We describe our analysis of the K2 photometry and of supplementary imaging and spectroscopic data in Sec. 2. In Sec. 3 we present the results of our analysis of

[1] Lunar & Planetary Laboratory, University of Arizona Lunar, 1629 E. University Blvd., Tucson, AZ, USA, ianc@lpl.arizona.edu
[2] Astronomy Department, University of California, Berkeley, CA, USA
[3] NASA Ames Research Center, Moffett Field, CA, USA
[4] Institute for Astronomy, University of Hawaii, 2680 Woodlawn Drive, Honolulu, HI, USA
[5] NASA Exoplanet Science Institute, California Institute of Technology,770 S. Wilson Ave., Pasadena, CA, USA
[6] Department of Physics & Astronomy, Georgia State University, Atlanta, GA, USA
[7] Max-Planck Institut für Astronomie, Königstuhl 17, Heidelberg, Germany
[8] Department of Physics, University of Notre Dame, 225 Nieuwland Science Hall, Notre Dame, IN, USA
[9] University of Hertfordshire, College Lane, AL10 9AB, Hatfield, UK
[10] Department of Physics & Astronomy, University of California Los Angeles, Los Angeles, CA, USA
[11] Department of Astronomy, Cornell University, 122 Sciences Drive, Ithaca, NY, USA
[11] NASA Postdoctoral Program Fellow

TABLE 1
Stellar Parameters of EPIC 201367065

Parameter	Value	Source
Identifying information		
α R.A. (hh:mm:ss)	11:29:20.388	
δ Dec. (dd:mm:ss)	-01:27:17.23	
2MASS ID	11292037-0127173	2MASS
Photometric Properties		
B (mag).....	13.52 ± 0.06	APASS
V (mag).....	12.17 ± 0.01	APASS
g (mag)	12.871 ± 0.030	APASS
r (mag)	11.582 ± 0.020	APASS
i (mag).....	10.98 ± 0.17	APASS
J (mag).....	9.421 ± 0.027	2MASS
H (mag)	8.805 ± 0.044	2MASS
Ks (mag)	8.561 ± 0.023	2MASS
W1 (mag)	8.443 ± 0.022	AllWISE
W2 (mag)	8.424 ± 0.019	AllWISE
W3 (mag)	8.322 ± 0.021	AllWISE
Spectroscopic and Derived Properties		
μ_α (mas yr^{-1})	88.3 ± 2.0	Zacharias et al. (2012)
$\mu\delta$ (mas yr^{-1})	-73.6 ± 2.7	Zacharias et al. (2012)
Barycentric rv (km s^{-1})	32.6 ± 1	APF, this paper
Distance (pc)	45 ± 3	this paper
EW (Hα) (Å)	-0.84Å	EFOSC, this paper
Age (Gyr)	$\gtrsim$1	EFOSC, this paper
Spectral Type	M0.2±0.3V	This paper.
[Fe/H]	-0.32 ± 0.13	uSpeX, this paper
$T_{\rm eff}$ (K)	3896 ± 189	uSpeX, this paper
M_* ($M_\odot$)	0.601 ± 0.089	uSpeX, this paper
R_* ($R_\odot$)	0.561 ± 0.068	uSpeX, this paper

EPIC 201367065's properties and discuss the potential for future observations of this and other systems discovered by K2.

2. OBSERVATIONS AND ANALYSIS

We identified the high proper motion star PMI11293-0127 as a target for our Campaign 1 proposal (GO1036[13], PI Crossfield) from the SUPERBLINK proper motion survey (Lépine & Shara 2005; Lépine & Gaidos 2011). We identified the star as a probable nearby M dwarf based on a color and proper motion selection scheme and selecting all targets with $(V-J) > 2.5$, $V + 5\log\mu + 5 < 10$, and $(6V - 7J - 3) < 5\log\mu$, where μ is the proper motion. The star matched the source EPIC 201367065 in the Kepler input catalog (Huber 2014). K2 then observed this target in long-cadence mode during C1, covering 30 May to 21 Aug 2014. Target properties are summarized in Table 1).

2.1. *K2 Photometry*

2.1.1. *Extracting the Photometry*

We extracted the photometry EPIC 201367065 from the pixel data, which we downloaded from the MAST. Because K2 only has two functional reaction wheels, the telescope cannot maintain the 50-millipixel pointing precision achieved during the prime mission. The dominant drift is roll around the telescope boresight. When the spacecraft reaches a pre-determined limit the spacecraft corrects this roll with a thruster fire. As the spacecraft rolls, stars move over different pixels having different sensitivities. Thus, motion of the star results in apparent changes in stellar brightness.

Because a target star traces out similar paths during each roll of the spacecraft, it is possible to separate out variations in stellar brightness that are roll angle dependent, and to remove these variations from the photometry. Our extraction pipeline draws heavily on the work of Vanderburg & Johnson (2014). We begin by computing the median flux for each frame and adopt this value as the background flux level. The background flux is subtracted out on a frame by frame basis. We compute the raw photometry, $F_{\rm SAP}$, by summing the flux within a soft-edged circular aperture centered around the target star. We compute the row and column centroids within the aperture.

On short timescales, spacecraft roll is the dominant motion term and can be described by a single variable. We identify the roll direction by computing the principle components of the row and column centroids, x' and y'. We fit for a function that relates $F_{\rm SAP}$ to x'. We describe this trend by $F_{\rm SAP} = {\rm GP}(x')$, where GP is a Gaussian process having a correlation matrix given by a squared exponential kernel. Fitting the GP(x') is an iterative process where outliers are identified and removed and the hyperparameters associated with the squared exponential kernel are adjusted to yield the minimum residual RMS.

The algorithm described in Vanderburg & Johnson (2014) was developed for the K2 engineering campaign (C0), where the time baseline was short enough that drifts in stellar position along the y' direction could be ignored. During 80 day period of C1 observations, stars moved enough along the y' direction that the GP(x') determined using data early in the campaign was no-longer an appropriate description of the position-dependent flux variations. Adopting an approach described in Vanderburg (2014), we divided the C1 observations in to six nearly equal segments and performed the 1D decorrelation approach described above on each segment individually. The entire procedure described above is repeated for different aperture radii (2, 3, 4, 5, 6, and 7 pixels). We select the aperture size that minimizes the calibrated RMS. For EPIC 201367065, a circular aperture with a 4 pixel radius yielded the best calibrated photometry (which is available as an electronic supplement to this paper). We see no convincing evidence of periodic modulation that might indicate stellar rotation.

2.1.2. *Transit Detection*

We searched through the calibrated and detrended photometry (shown in Fig. 1a) using the TERRA algorithm described in Petigura et al. (2013). TERRA identified a transit candidate having $P = 10.056$ days and SNR = 59. We fit this candidate with a Mandel & Agol (2002) model and subtracted the best fit model from the photometry. We reran TERRA on the photometry with the $P = 10.056$ day candidate removed. We found a second candidate having $P = 24.641$ days and SNR = 30. Again we removed the best-fitting model. TERRA did not find any additional transits, but a ∼45-day candidate was identified by eye (TERRA currently requires 3 detected transits, and thus was not sensitive to the longest period candidate which only transits twice during C1). We fit each of these two transits individually and find

[13] The star was also identified in programs GO1006, GO1050, GO1052, GO1036, GO1075, GO1059, and GO1063.

consistent transit parameters, supporting the hypothesis that they result from a single planet. At half of this period a third transit would occur in C1's data gap (see Fig. 1), but this would give the outer two planets a period ratio of just 1.1. The previous record-holder for a close period ratio is the Kepler-36 system (Carter et al. 2012; Winn & Fabrycky 2014), whose two planets exhibit a considerably larger period ratio of 1.17 and transit timing variations of many hours. It is unlikely that such an unusual system would lie just 45 pc away, so we conclude that the third planet's period is ∼45 d.

2.2. *Stellar Spectroscopy & Validation*

We observed EPIC 201367065 using several spectrographs to constrain the stellar properties. These observations are described below. The reduced spectra are attached as an electronic supplement to this paper, and the the derived parameters are listed in Table 1.

2.2.1. *Observations and Reduction*

We obtained $R \sim 1500$ spectra from 0.6–1.0μm of EPIC 201367065 and a number of calibration objects using NTT/EFOSC2 (Buzzoni et al. 1984) on UT 11 Jan 2015 as part of 70-night K2 followup program (PID 194.C-0443, PI Crossfield). We draw our calibrators from several recent works (Boyajian et al. 2012; Pecaut & Mamajek 2013; Mann et al. 2013a). A forthcoming paper will discuss these efforts; in brief, we bias-subtract and flat-field the data frames, extract spectra using IRAF, and wavelength-calibrate using EFOSC2's internal HeAr lamps. We achieve a S/N per resolution element of ∼100 for EPIC 201367065 and somewhat higher for our reference sample. We flux-calibrate the extracted spectrum using observations of spectrophotometric standards.

We observed EPIC 201367065 on 2015 January 11 UT using the uSpeX spectrograph (Rayner et al. 2003) on the 3.0m NASA Infrared Telescope Facility (IRTF). The data were taken under near-photometric conditions with an average seeing of ∼0.″7. We observed with the instrument in short cross dispersed mode (SXD) using the 0.3 X 15" slit. This setup provides simultaneous wavelength coverage from 0.7 to 2.5 μm at a resolution of R≈2000. The extended blue wavelength coverage is a result of the recent chip upgrade SpeX received in July 2014 (now called uSpeX). The target was placed at two positions along the slit and observed in an ABBA pattern for subsequent sky subtraction. The observing sequence consisted of 8 × 40 s exposures for a total integration time of 320s. Once the exposures were stacked, this integration time led to a signal-to-noise of > 140 per resolution element. We obtained standard uSpeX calibration frames consisting of flats and arclamp exposures immediately before observing EPIC 201367065.

The uSpeX spectrum was reduced using the SpeXTool software package (Cushing et al. 2004). SpeXTool performs flat-field correction and wavelength calibration from the calibration frames followed by sky subtraction and extraction of the one-dimensional spectrum. Individual exposures of the target were combined using the *xcombspec* routine within SpeXTool. We corrected for atmospheric absorption and performed flux calibration using the A0V-type star HD 97585 which was observed within 20 minutes and 0.015 airmass of the target. A telluric correction spectrum was constructed from the spectrum of the A0V using the *xtellcor* package (Vacca et al. 2003) and applied to the spectrum of EPIC 201367065. This package also performs flux calibration. Separate, telluric-corrected uSpeX orders were combined and flux matched into a continuous spectrum using the *xmergeorders* routine. To minimize errors in the spectral slope due to changes in seeing, guiding, and differential refraction, we aligned the slit with the parallactic angle and minimized the time between observations of the target and standard star. Prior to performing any spectroscopic analyses, we also applied corrections for the barycentric velocity of the observatory and the measured radial velocity. The final, calibrated spectrum is shown in Fig. 2.

2.2.2. *Stellar Parameters*

Mann et al. (2013b) motivate a set of temperature sensitive spectral indices spanning the visible, J-, H-, and K-bands that are calibrated using the M dwarf sample of Boyajian et al. (2012) with interferometrically measured radii. We used these indices to estimate the temperature of EPIC 201367065. We calculate the mean of the temperatures from each of the three band indices and their rms scatter and find $T_{\rm eff}$ = 3896±117 K (±148 K systematic error, ±189 K total error). This effective temperature is consistent with that of a main-sequence M0 dwarf (Pecaut & Mamajek 2013) and is thus consistent with our determinations of the star's spectral type.

We adopt the metallicity calibration of Mann et al. (2013a) to remain consistent with our methods for determining $T_{\rm eff}$, and other parameters. We use custom IDL software provided by A. Mann[14] to calculate the metallicity in in the visible, J-, H-, and K-bands following the calibrations of Mann et al. (2013a). Since our uSpeX spectrum does not extend < 0.7 μm, we do not use the visible band calibrations. Following the suggestion of Mann et al. (2013a), we also discard the J-band metallicity, which is often an outlier. Our final metallicity is the mean of those measured from the H- and K-band relations and the error is the quadrature sum of the measurement error and systematic error in each band. We find [Fe/H] = -0.32±0.13. Thus, EPIC 201367065's metallicity is sub-solar, broadly consistent with many other nearby, field-age, M dwarfs.

Mann et al. (2013b) provide empirical calibrations to calculate the radii, masses, and luminosities given the $T_{\rm eff}$ of an M dwarf. We estimate these additional fundamental parameters again using IDL software written by A. Mann[15] to calculate radius, mass, and luminosity and their associated errors using the relations detailed in Mann et al. (2013a). Using the most conservative $T_{\rm eff}$ errors, we calculate $R_* = 0.561\pm0.068\ R_\odot$ and $M_* = 0.601\pm0.089\ M_\odot$. These values, and the other fundamental parameters of the star, are tabulated in Table 1 and are used for subsequent estimates of the individual planet properties.

Independent of these parameters, we also assign a spectral type to this star using molecular band heads in our optical and NIR spectra. The TiO5 and CaH3 indices (Reid et al. 1995; Gizis 1997) are calibrated for the earliest M dwarfs (Lépine et al. 2003) and avoid regions of

[14] `https://github.com/awmann/metal`
[15] `https://github.com/awmann/Teff_rad_mass_lum`

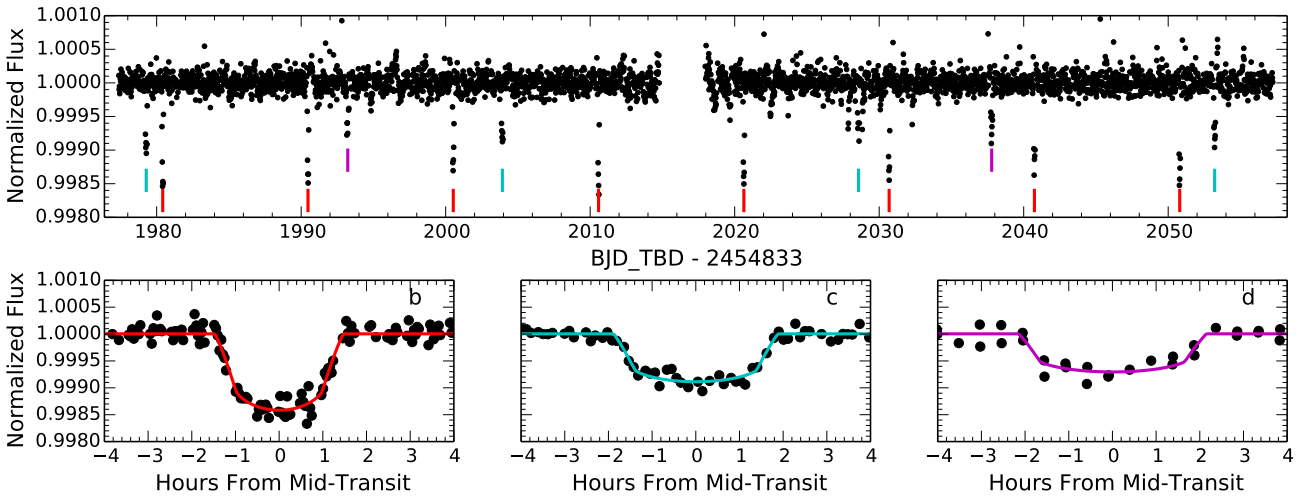

FIG. 1.— *Top*: Calibrated K2 photometry for EPIC 201367065. Vertical ticks indicate the locations of each planets' transits. *Bottom*: Phase-folded photometry and best-fit light curves for each planet.

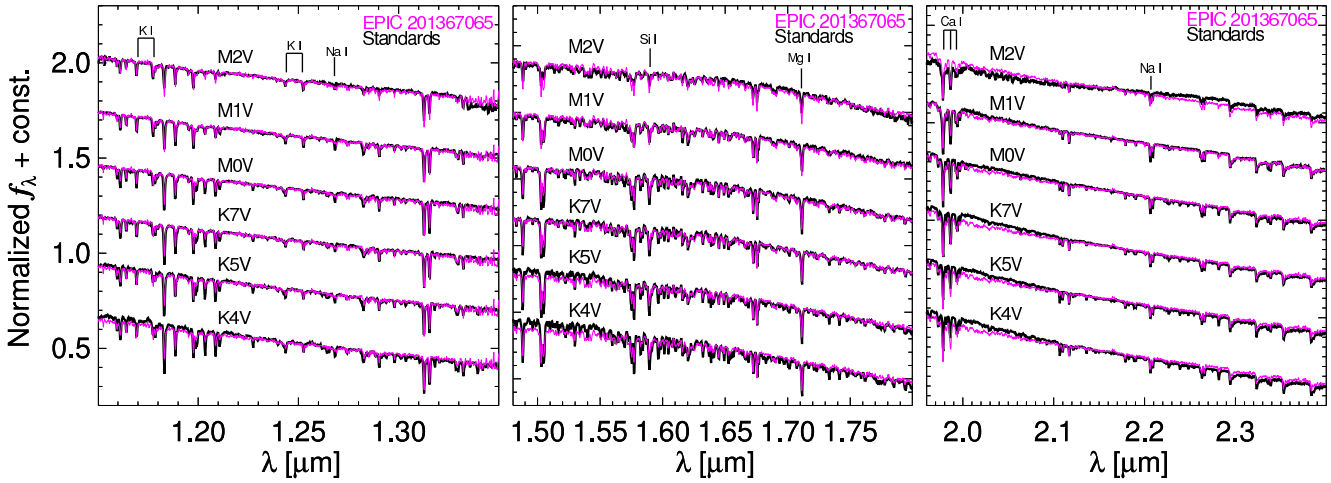

FIG. 2.— Calibrated IRTF/uSpeX spectra of our target compared to spectral standards. Stellar parameters are tabulated in Table 1.

the spectrum with heavy telluric contamination. Following the index definitions and spectral type relations of Lépine et al. (2003) and accounting for the relation's intrinsic accuracy, our EFOSC spectrum yields a spectral type of K7.7±0.5 and our uSpeX spectrum yields M0.3±0.5. Rojas-Ayala et al. (2012) define the H_2O-K2 NIR spectral type index to estimate M dwarf types from NIR spectra using the slope of the K-band continuum. We calculate this index from our uSpeX spectrum and estimate a spectral type of M0.7±0.6, where we adopt the systematic error from the index-spectral type relation. This NIR type is consistent with the type from the EFOSC and uSpeX red optical data and also with the original photometric estimate. We adopt the weighted mean of the spectroscopic values, giving a spectral type of M0.2±0.3V. Using the $riJHK$ photometric calibrations of Kraus & Hillenbrand (2007), we estimate a distance to EPIC 201367065 of 45 ± 3 pc.

We obtained high-resolution (2" slit width with the B decker) spectra of EPIC 201367065 with the Levy Spectrometer (Radovan et al. 2010) on the Automated Planet Finder (APF) telescope (Vogt et al. 2014). The spectra were reduced using standard procedures, as described in (Fulton 2015). Inspection of the gravity-sensitive lines confirms that EPIC 201367065 is a high gravity target, consistent with the medium resolution spectra described above. We do not see any evidence of a second set of spectral lines, ruling out companions ∼2.5 mag fainter than EPIC 201367065 at visible wavelengths.

2.2.3. *Activity, Age, and Membership*

Lines in the Balmer series are associated with magnetic activity in late-type stars. The strongest line in the series, Hα at 6563 Å, is classically used to asses the activity of M dwarfs and as a crude indicator of age (West et al. 2004, 2008). We therefore measure the Hα equivalent width (EW) as defined by West et al. (2011) and find EW < 0.75 Å, indicating that EPIC 201367065 is an inactive star. This lack of activity in an M0 dwarf is indicative of a field age and translates to a lower age limit of ∼1 Gyr (West et al. 2008).

We assessed the nearby young moving group member-

ship using the BANYAN II web tool (Malo et al. 2013; Gagné et al. 2014), which calculates the membership probability using Bayesian inference and the proper motion, sky coordinates, radial velocity and distance. The probability of our object being a member one any known nearby young moving groups is $< 0.1\%$, given the sky coordinates, proper motion and radial velocity. In order to further rule out possible young moving group membership we also used our photometric distance and assumed a conservative 20% distance uncertainty. After including the photometric distance in the BANYAN II web tool, the young moving group membership probability was still $< 0.1\%$. We also compared the heliocentric space positions and kinematics with those of the known young moving groups, confirming the Banyan II results. Thus we conclude that our object is unlikely to be a member of any nearby young moving groups.

2.3. *Archival and Adaptive Optics Imaging*

To rule out the presence of a background star being the source of or diluting the transit events, we compare two epochs of imaging data from the Digitized Sky Survey (DSS) and the Sloan Digital Sky Survey (SDSS) separated by 45 years. The data shown in Fig. 3 are the DSS-Red plates with a pixel scale of $1.7''$/pixel taken on 19 April 1955 and the SDSS r-band image with a pixel scale of $0.396''$/pixel taken on 03 March 2000. The images are 1 arcminute on a side and clearly show the proper motion of the primary target. The nearby star located $27''$ to the NE is consistent with zero motion within our astrometric uncertainties; this star lies outside the photometric aperture applied to the K2 photometry. The primary target, in contrast, displays a clear proper motion of $6.2''$ over 45 years, in reasonable agreement with the measured proper motion (Lépine & Gaidos 2011; Zacharias et al. 2012). In the DSS image there is no evidence of a background star, and we estimate if a star is located at the position of the primary target in the Kepler data, that star must be at least 6 magnitudes (or more) fainter than the target star.

Near-infrared adaptive optics imaging of EPIC 201367065 was obtained at Keck Observatory on the night of 2015 January 12 UT. Observations were obtained with the 1024×1024 NIRC2 array and the natural guide star system; the target star was bright enough to be used as the guide star. The data were acquired in the narrow-band K-band continuum filter (Kcont) using the narrow camera field of view with a pixel scale of 9.942 mas pix^{-1}. A 3-point dither pattern was utilized to avoid the noisier lower left quadrant of the NIRC2 array. One additional frame was obtained from a dither pattern with two failed frames. Each position was observed with 10 coadds and a 1.5 s integration time for a total of 60 seconds of on-source exposure time. The data were flatfielded and sky subtracted and the dither positions were shifted and coadded into a single final image, shown in Fig. 3b.

The target star was measured with a resolution of $0.07''$ (FWHM) and no other stars were detected within the $10''$ field of view of the camera. The data are sensitive to stars that have K-band brightness of $\Delta K = 2.4$ mag at a separation of $0.07''$ and $\Delta K = 6.5$ mag at a separation of $0.5''$ from the central star. The sensitivities were estimated by injecting simulated sources, with a signal-to-noise of 5, into the final combined images at distances of N*FWHM from the central source. The 5σ sensitivities, as a function of radius from the star, are shown in Fig. 3a.

2.4. *Light Curve Fitting*

We analyze the photometry using standard Python-based minimizers, the `emcee` Markov Chain Monte-Carlo (MCMC) package (Foreman-Mackey et al. 2013), and the JKTEBOP lightcurve code (Southworth et al. 2004; Southworth 2011) using numerical integration to account for our ∼30-min cadence. We fit each planet's transit separately, after first masking out data taken during the other planets' transits.

We use the best-fit TERRA parameters to initialize the fits. We assumed a linear limb-darkening relation for the star. Because the data are insufficient to break all degeneracies between the light curve parameters (Muirhead et al. 2012), we impose Gaussian priors in our analysis. For the limb-darkening parameter u, we assume a distribution with center 0.560 and dispersion 0.044; these values correspond to the mean and standard deviation, respectively, of all linear limb-darkening terms tabulated by (Claret et al. 2012) that satisfy $3300 \leq T_{eff} \leq 3700$ K and $\log_{10} g \geq 4.5$. Using the spectroscopic parameters presented below (Table 1), we also impose a prior on the stellar density to constrain R_*/a (Seager & Mallén-Ornelas 2003). This last point assumes that the planets' orbits are circular, an assumption that future RV measurements will test.

We seed our 60 MCMC chains with values near the best-fit parameters. We assign our data points equal weights, such that the best-fit likelihood equals $-\chi^2/2$. After burn-in we run the MCMC sampler: after each set of 2000 steps, we optimize the fits given by each chain's parameters to check for better fits to the data. We re-initialize the sampler and re-scale the data weights if we find an improved fit, repeating until all parameters' chains are well-mixed (as indicated by Gelman-Rubin metrics ≤ 1.03; Gelman & Rubin 1992). As our final confidence intervals, we use the 15.87% and 84.13% percentiles of each parameters' posterior distribution. The final distributions are unimodal. Fig. 1 shows the resulting photometry and best-fit models, and Table 2 summarizes the final values and uncertainties.

2.5. *Ruling Out False Positives*

Almost all candidates in *Kepler*'s multi-planet systems are *bona fide* planets (Lissauer et al. 2011), but one pernicious source of confusion is the possibility of mistaking blended stars each hosting their own planets for a single multi-planet system. We therefore investigated the possibility that EPIC 201367065 might be a blend of multiple stars. First, we note that EPIC 201367065's proper motion (listed in Table 1) is large enough that optical DSS survey images reveal no objects at the star's current location (see Fig. 3). Blends involving background eclipsing binaries are thus immediately excluded.

The remaining possible configuration involves a late-type M dwarf close to EPIC 201367065 and with its own transiting planet(s), but this is extremely unlikely. An M4 dwarf would have $\Delta K_p \approx 2.7$ and so might be missed in our APF and EFOSC spectra, but the M4 would have $\Delta K_s \approx 2.0$ (Kraus & Hillenbrand 2007) and so must lie at $a \lesssim 2.8$ AU while still needing to host its own $2R_\oplus$

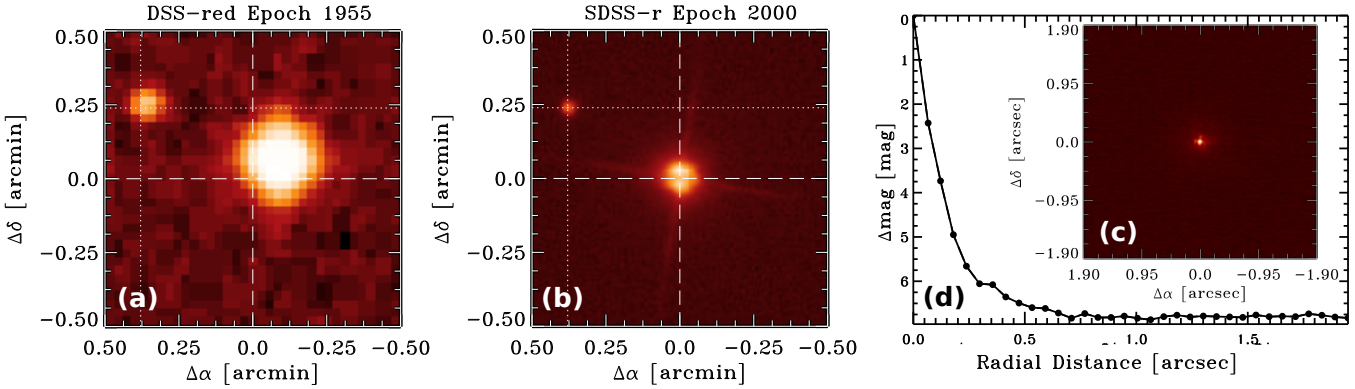

FIG. 3.— We detect no objects within 25" of EPIC 201367065: (a) in the DSS; (b) in SDSS; (c) with Keck/NIRC2 K-band adaptive optics. (d) K_s-band contrast curve indicating Keck/NIRC2's sensitivity to faint nearby companions.

transiting planet. As an example: the likelihood that EPIC 201367065 has a low-mass companion is ∼0.4 and that such a companion would lie at a projected separation > 2.8 AU is ∼0.5 (Duchêne & Kraus 2013). For planet b, the likelihood of an M dwarf hosting such a planet is $\lesssim 0.15$ (Dressing & Charbonneau 2013); and the likelihood of it transiting is ∼0.02. Then the likelihood of such a contrived configuration is just $\sim 6 \times 10^{-4}$ (1 in 1700), so we eliminate this scenario as well. We therefore conclude that EPIC 201367065 indeed hosts a three-planet system.

2.6. *System Stability*

Here we investigate the dynamical stability of the three-planet EPIC 201367065 system. The planet masses are unconstrained by transit photometry, so we adopt the following mass-radius relationship:

- $M = \frac{4\pi}{3} R^3 \rho$, where $\rho = (2.43 + 3.39 * (R_P/R_\oplus))$ g cm^{-3} for $R_P < 1.5 R_\oplus$ (Weiss & Marcy 2014)
- $M = 2.69 M_\oplus \left(\frac{R_P}{R_\oplus}\right)^{0.93}$ (Weiss & Marcy 2014) for $1.5 R_\oplus < R_P < 4.0 R_\oplus$
- $M = M_\oplus \left(\frac{R_P}{R_\oplus}\right)^{2.06}$ for $R_P > 4.0 R_\oplus$ (Lissauer et al. 2012)

Adopting the above mass-radius relationship we derive masses of 5.3, 4.3, and 4.4 $M_\oplus$ for planets b, c, and d respectively. We integrate the system forward in time with the Mercury integration package (Chambers 1999) utilizing the hybrid integrator and found the system to be stable for the full 2×10^5 yr simulation.

We also evaluate analytically the system's stability. The relevant length scale for dynamical interactions between planets is the mutual Hill radius:

$$R_H = \left[\frac{M_{\rm in} + M_{\rm out}}{3 M_\star}\right]^{1/3} \frac{a_{\rm in} + a_{\rm out}}{2} \qquad (1)$$

where M and a denote mass and semi-major axis, respectively. The subscripts "in" and "out" correspond to the inner an outer planets respectively. Following Fabrycky et al. (2012), for each pair of planets, we compute $\Delta = (a_{\rm out} - a_{\rm in})/R_H$, the separation between the planets measured in units of their mutual Hill radii. If two planets begin on circular orbits, they are stable indefinitely if $\Delta > 2\sqrt{3} \approx 3.5$ Gladman (1993). In the case of EPIC 201367065, $\Delta_{\rm bc} = 15.9$ and $\Delta_{\rm cd} = 11.0$. Thus, the two pairs of adjacent planets do not violate the criterion of Hill stability.

There is no analytic stability criterion for systems having three or more planets Fabrycky et al. (2012). Fabrycky et al. (2012) introduce $\Delta_{\rm in} + \Delta_{\rm out}$, as a heuristic metric for assessing the stability of three planets in triple or higher multiplicity systems. They adopt $\Delta_{\rm in} + \Delta_{\rm out} > 18$ as a heuristic criterion for the stability of three planets, motivated by suites of direct numerical integrations (e.g. Smith & Lissauer (2009)). This criterion is empirically supported by the ensemble of systems with three or more transiting planets from the Kepler mission. Among the 413 such systems in Fabrycky et al. (2012), only six had $\Delta_{\rm in} + \Delta_{\rm out} < 18$. For EPIC 201367065, $\Delta_{\rm bc} + \Delta_{\rm cd} = 26.9$, and thus has a similar architecture to the ensemble of triple and higher systems discovered during the prime Kepler mission.

We can also assess the implications of a false positive interpretation on the stability of these planets. If EPIC 201367065 is a binary star system, with transiting planets around the fainter secondary, the true radii of the planets are larger than reported in this work, because their depths are diluted by the primary star. Larger radii imply larger masses meaning the system sits closer to the stability limit. We explored how much larger the planets can be before they violate Hill-stability. The three panels of Fig. 4 show how $\Delta_{\rm bc}$, $\Delta_{\rm cd}$, and $\Delta_{\rm bc} + \Delta_{\rm cd}$behave as we increase the planet radii by a multiplicative scale factor. As before, masses are computed according to the mass-radius relationship introduced above. The two planet stability limit does not impose a tight constraint on the range of plausible planet sizes. Radii may be scaled up by a factor of 7 before the two planet stability limit is violated. However, planet radii may only be scaled up by a factor of 2.5 before the three-planet stability limit is violated. This corresponds to rough upper limits on the masses of planets b,c, and d of 30, 19, 9.1 $M_\oplus$respectively.

3. DISCUSSION

Our analysis indicates three small planets orbiting this bright, nearby M dwarf. The planets range in size from $2 R_\oplus$ to $1.5 R_\oplus$, indicating that they may span the gap between rock-dominated "Earths"/"super-Earths" and low-density "sub-Neptunes" with considerable volatile

TABLE 2
Planet Parameters

Parameter	Units	b	c	d
T_0	$BJD_{TDB} - 2454833$	$1980.4189^{+0.0011}_{-0.0011}$	$1979.2786^{+0.0026}_{-0.0027}$	$1993.2232^{+0.0037}_{-0.0043}$
P	d	$10.05403^{+0.00026}_{-0.00025}$	$24.6454^{+0.0013}_{-0.0013}$	$44.5631^{+0.0063}_{-0.0055}$
i	deg	$89.28^{+0.46}_{-0.60}$	$89.55^{+0.29}_{-0.44}$	$89.68^{+0.21}_{-0.26}$
R_P/R_*	%	$3.483^{+0.123}_{-0.070}$	$2.786^{+0.143}_{-0.083}$	$2.48^{+0.14}_{-0.10}$
T_{14}	hr	$2.553^{+0.047}_{-0.044}$	$3.428^{+0.106}_{-0.097}$	$3.98^{+0.17}_{-0.15}$
R_*/a	–	$0.0343^{+0.0049}_{-0.0020}$	$0.0193^{+0.0041}_{-0.0014}$	$0.0127^{+0.0025}_{-0.0010}$
b	–	$0.37^{+0.22}_{-0.23}$	$0.41^{+0.26}_{-0.25}$	$0.45^{+0.23}_{-0.28}$
u	–	$0.560^{+0.041}_{-0.042}$	$0.557^{+0.043}_{-0.044}$	$0.563^{+0.041}_{-0.042}$
a	AU	$0.0769^{+0.0036}_{-0.0040}$	$0.1399^{+0.0066}_{-0.0073}$	$0.2076^{+0.0098}_{-0.0108}$
R_P	$R_\oplus$	$2.14^{+0.27}_{-0.26}$	$1.72^{+0.23}_{-0.22}$	$1.52^{+0.21}_{-0.20}$
$S_{\rm inc}$	$S_\oplus$	$11.0^{+4.1}_{-3.1}$	$3.32^{+1.25}_{-0.95}$	$1.51^{+0.57}_{-0.43}$

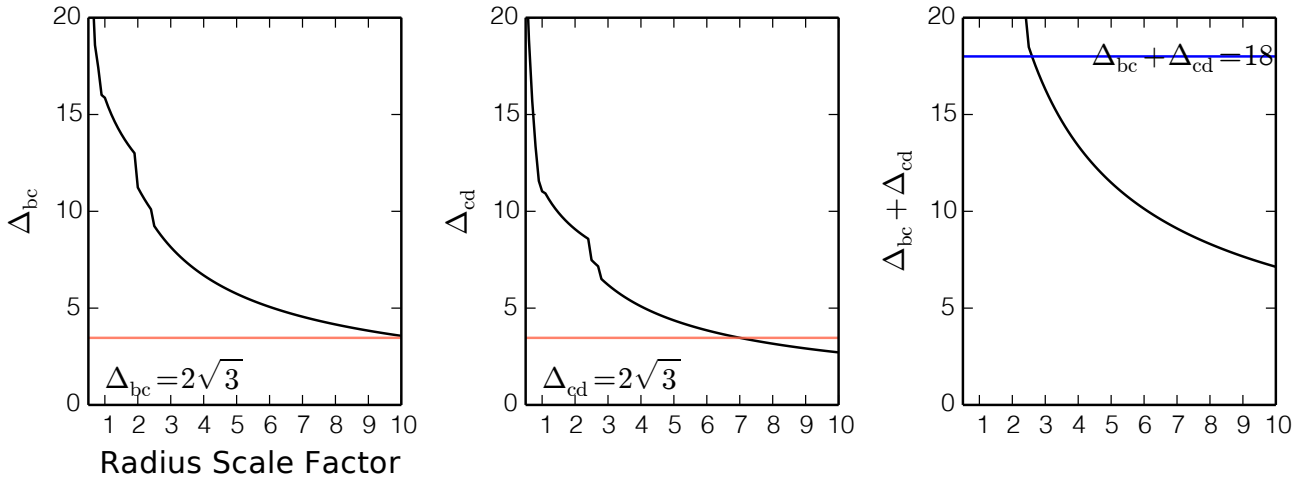

Fig. 4.— The left and center panel plot Δ for the bc and cd pairs while the radii are adjusted by a multiplicative scale factor. The red line shows denotes the two planet stability limit, below which pairs are not Hill-stable. Both pairs of planets are stable according, even if all planets were 7× larger and correspondingly more massive. The right panel shows the sum Δ computed for each pair, again when radii are adjusted according to a scale factor. The blue line shows the three-planet heuristic stability criterion adopted in Fabrycky et al. (2012). EPIC 201367065 is stable according to the three planet stability limit.

content (Marcy et al. 2014; Rogers 2014; Dressing et al. 2014).

The planets' radii imply masses of roughly 4–5 M_E and Doppler amplitudes of 1.2–2.3 $\rm m\,s^{-1}$, within reach of modern RV spectrographs. These mass estimates assume that the planets fall on the mean mass-radius relationship, characterized by high densities and rocky compositions for planets smaller than ∼1.6 R_E. However, most of the planets with measured masses and $R_p < 1.6R_E$ have high incident fluxes (e.g., Batalha et al. 2011; Howard et al. 2013; Pepe et al. 2013). The mass-radius relationship is poorly constrained for cool planets that are less likely to be sculpted by thermal evolution and photo-evaporation (Lopez et al. 2012). Characterizing the mass-radius relationship for these cool, small planets is an important step to learning whether Earth-size planets in the habitable zone also have Earth-like atmospheres.

The planets' receive insolation levels ($S_{\rm inc}$) roughly 11, 3.3, and 1.5× that of the Earth for planets b, c, and d, respectively. Planet d is located at the inner edge of the system's habitable zone, with $S_{\rm inc} = 1.51^{+0.57}_{-0.47} S_\oplus$ – close to the limits of the empirical habitable zone (e.g., Kopparapu et al. 2014)– making this planet a very interesting potential super-Venus or super-Earth. Because this system is so close the atmosphere of this planet can be explored in the near future; depending on atmospheric, cloud, and surface properties liquid water could potentially persist on planet c (Zsom et al. 2013, but see Kasting et al. 2014).

The EPIC 201367065 system is a convenient system to measure the atmospheric properties of small, cool planets. Indeed, the star is a full magnitude brighter than Kepler-138 (Kipping et al. 2014), the previous best system for characterizing cool, nearly Earth-size planets. For cloud-free, hydrogen-dominated atmospheres, we estimate that these planets will show spectral features with amplitudes of $10HR_p/R_\star^2$ on the order of 100–200 ppm (Miller-Ricci et al. 2009), where H is the atmospheric scale height. These features would be detectable with current instrumentation on the Hubble Space Telescope (Kreidberg et al. 2014). Transit features in a heavy atmo-

sphere (e.g., N_2, CO_2) would be an order of magnitude smaller, and secondary eclipses will have depths on the order of $(R_p/R_\star)^2 T_{\rm eq}/T_\star \sim 50$–$150$ ppm – either of these scenarios should be detectable with JWST. By allowing us to measure masses and atmospheric conditions for 3 small planets in a single system, EPIC 201367065 represents an exciting opportunity to test theories of planet formation and evolution in a single extrasolar laboratory.

That K2 should reveal such a system in its first full campaign demonstrates that the mission will extend *Kepler*'s compelling scientific legacy for years to come. Along with HIP 116454 (Vanderburg et al. 2014), the discovery of EPIC 201367065 shows that K2 is already finding fascinating new targets for observation with JWST and heralds an era of further unprecedented discoveries in the *TESS* era.

Acknowledgements We thank Geoff Marcy, Evan Sinukoff, and Charles Beichman for helpful conversations, Vishnu Reddy for swapping SpeX time, and Lauren Weiss for initiating robotic observations with the APF Telescope. A. W. H. acknowledges NASA grant NNX12AJ23G, and S.L. acknowledges NSF grant AST 09-08419. This work made use of the SIMBAD database (operated at CDS, Strasbourg, France), NASA's Astrophysics Data System Bibliographic Services, and the Authorea collaborative writing website. This research has made use of the NASA Exoplanet Archive and the Infrared Science Archive, which are operated by the California Institute of Technology, under contract with the National Aeronautics and Space Administration. Portions of this work were performed at the California Institute of Technology under contract with the National Aeronautics and Space Administration. Some of the data presented herein were obtained at the W.M. Keck Observatory (which is operated as a scientific partnership among Caltech, UC, and NASA) and at the Infrared Telescope Facility (IRTF, operated by UH under Cooperative Agreement no. NNX-08AE38A with NASA, Science Mission Directorate, Planetary Astronomy Program). The authors wish to recognize and acknowledge the very significant cultural role and reverence that the summit of Mauna Kea has always had within the indigenous Hawaiian community. We are most fortunate to have the opportunity to conduct observations from this mountain.

Facility: Kepler, K2, IRTF (SPEX), NTT (EFOSC2), APF (Levy), Keck-II (NIRC2)

REFERENCES

????
08. 1
Batalha, N., Kalirai, J., Lunine, J., Clampin, M., & Lindler, D. 2013, Transiting Exoplanet Simulations with the James Webb Space Telescope, Tech. rep.
Batalha, N. M., Borucki, W. J., Bryson, S. T., et al. 2011, ApJ, 729, 27
Beichman, C., Benneke, B., Knutson, H., et al. 2014, arXiv:1411.1754
Boyajian, T. S., von Braun, K., van Belle, G., et al. 2012, ApJ, 757, 112
Buzzoni, B., Delabre, B., Dekker, H., et al. 1984, The Messenger, 38, 9
Carter, J. A., Agol, E., Chaplin, W. J., et al. 2012, Science, 337, 556
Chambers, J. E. 1999, MNRAS, 304, 793
Claret, A., Hauschildt, P. H., & Witte, S. 2012, A&A, 546, A14
Cushing, M. C., Vacca, W. D., & Rayner, J. T. 2004, PASP, 116, 362
Dressing, C. D., & Charbonneau, D. 2013, ApJ, 767, 95
Dressing, C. D., Charbonneau, D., Dumusque, X., et al. 2014, arXiv:1412.8687
Duchêne, G., & Kraus, A. 2013, ARA&A, 51, 269
Fabrycky, D. C., Ford, E. B., Steffen, J. H., et al. 2012, ApJ, 750, 114
Foreman-Mackey, D., Hogg, D. W., Lang, D., & Goodman, J. 2013, PASP, 125, 306
Fulton, Weiss, S. e. a. 2015, ApJ, submitted
Gagné, J., Lafrenière, D., Doyon, R., Malo, L., & Artigau, É. 2014, ApJ, 783, 121
Gelman, A., & Rubin, D. B. 1992, Statistical Science, 7, 457
Gizis, J. E. 1997, AJ, 113, 806
Gladman, B. 1993, Icarus, 106, 247
Hansen, B. M. S. 2014, arXiv:1403.6553
Howard, A. W., Marcy, G. W., Johnson, J. A., et al. 2010, Science, 330, 653
Howard, A. W., Marcy, G. W., Bryson, S. T., et al. 2012, ApJS, 201, 15
Howard, A. W., Sanchis-Ojeda, R., Marcy, G. W., et al. 2013, Nature, 503, 381
Howell, S. B., Sobeck, C., Haas, M., et al. 2014, PASP, 126, 398
Huber, D. 2014, K2: Extending Kepler's Power to the Ecliptic. Ecliptic Plane Input Catalog, Tech. rep.
Kaltenegger, L., Segura, A., & Mohanty, S. 2011, ApJ, 733, 35
Kaltenegger, L., & Traub, W. A. 2009, ApJ, 698, 519
Kasting, J. F., Kopparapu, R., Ramirez, R. M., & Harman, C. E. 2014, Proceedings of the National Academy of Science, 111, 12641
Kipping, D. M., Nesvorný, D., Buchhave, L. A., et al. 2014, ApJ, 784, 28
Kopparapu, R. K., Ramirez, R. M., SchottelKotte, J., et al. 2014, ApJ, 787, L29
Kraus, A. L., & Hillenbrand, L. A. 2007, AJ, 134, 2340
Kreidberg, L., Bean, J. L., Désert, J.-M., et al. 2014, Nature, 505, 69
Lépine, S., & Gaidos, E. 2011, AJ, 142, 138
Lépine, S., & Shara, M. M. 2005, AJ, 129, 1483
Lépine, S., Shara, M. M., & Rich, R. M. 2003, AJ, 126, 921
Lissauer, J. J., Fabrycky, D. C., Ford, E. B., et al. 2011, Nature, 470, 53
Lissauer, J. J., Marcy, G. W., Rowe, J. F., et al. 2012, ApJ, 750, 112
Lopez, E. D., Fortney, J. J., & Miller, N. 2012, ApJ, 761, 59
Malo, L., Doyon, R., Lafrenière, D., et al. 2013, ApJ, 762, 88
Mandel, K., & Agol, E. 2002, ApJ, 580, L171
Mann, A. W., Brewer, J. M., Gaidos, E., Lépine, S., & Hilton, E. J. 2013a, AJ, 145, 52
Mann, A. W., Gaidos, E., & Ansdell, M. 2013b, ApJ, 779, 188
Marcy, G. W., Isaacson, H., Howard, A. W., et al. 2014, ApJS, 210, 20
Miller-Ricci, E., Seager, S., & Sasselov, D. 2009, ApJ, 690, 1056
Muirhead, P. S., Johnson, J. A., Apps, K., et al. 2012, ApJ, 747, 144
Pecaut, M. J., & Mamajek, E. E. 2013, ApJS, 208, 9
Pepe, F., Cameron, A. C., Latham, D. W., et al. 2013, Nature, 503, 377
Petigura, E. A., Howard, A. W., & Marcy, G. W. 2013, Proceedings of the National Academy of Science, 110, 19273
Radovan, M. V., Cabak, G. F., Laiterman, L. H., Lockwood, C. T., & Vogt, S. S. 2010, in Society of Photo-Optical Instrumentation Engineers (SPIE) Conference Series, Vol. 7735, Society of Photo-Optical Instrumentation Engineers (SPIE) Conference Series, 4
Rayner, J. T., Toomey, D. W., Onaka, P. M., et al. 2003, PASP, 115, 362
Reid, I. N., Hawley, S. L., & Gizis, J. E. 1995, AJ, 110, 1838
Rodler, F., & López-Morales, M. 2014, ApJ, 781, 54
Rogers, L. A. 2014, arXiv:1407.4457

Rojas-Ayala, B., Covey, K. R., Muirhead, P. S., & Lloyd, J. P. 2012, ApJ, 748, 93
Seager, S., & Mallén-Ornelas, G. 2003, ApJ, 585, 1038
Smith, A. W., & Lissauer, J. J. 2009, Icarus, 201, 381
Southworth, J. 2011, MNRAS, 417, 2166
Southworth, J., Maxted, P. F. L., & Smalley, B. 2004, MNRAS, 351, 1277
Stevenson, K. B., Harrington, J., Nymeyer, S., et al. 2010, Nature, 464, 1161
Swift, J. J., Johnson, J. A., Morton, T. D., et al. 2013, ApJ, 764, 105
Vacca, W. D., Cushing, M. C., & Rayner, J. T. 2003, PASP, 115, 389
Vanderburg, A. 2014, arXiv:1412.1827
Vanderburg, A., & Johnson, J. A. 2014, PASP, 126, 948
Vanderburg, A., Montet, B. T., Johnson, J. A., et al. 2014, arXiv:1412.5674, arXiv:1412.5674
Vogt, S. S., Radovan, M., Kibrick, R., et al. 2014, PASP, 126, 359
Weiss, L. M., & Marcy, G. W. 2014, ApJ, 783, L6
West, A. A., Hawley, S. L., Bochanski, J. J., et al. 2008, AJ, 135, 785
West, A. A., Hawley, S. L., Walkowicz, L. M., et al. 2004, AJ, 128, 426
West, A. A., Morgan, D. P., Bochanski, J. J., et al. 2011, AJ, 141, 97
Winn, J. N., & Fabrycky, D. C. 2014, ArXiv e-prints, arXiv:1410.4199
Zacharias, N., Finch, C. T., Girard, T. M., et al. 2012, VizieR Online Data Catalog, 1322, 0
Zsom, A., Seager, S., de Wit, J., & Stamenković, V. 2013, ApJ, 778, 109